

Fundamental mechanism of the creation of chemical bimodality in the Milky Way disc in the cold accretion theory

Masafumi Noguchi¹★

¹*Astronomical Institute, Tohoku University, 6-3, Aramaki, Aoba-ku, Sendai, Miyagi, 980-8578, Japan*

Accepted XXX. Received YYY; in original form ZZZ

ABSTRACT

Chemical bimodality of the Milky Way (MW) disc stars constitutes one of the most remarkable properties of MW. The cold accretion theory for the cosmological gas accretion provides one viable explanation to this phenomenon. In this scenario, the rapid cold-mode accretion in the early epoch creates the first generation stars relatively rich in α -elements (O, Mg, Si, S, Ca, etc) and later cooling flow produces iron-rich second generation stars, creating the bimodality in the $[\alpha/\text{Fe}]$ ratio. We employ a cosmologically motivated chemical evolution model for disc galaxies to elucidate the role played by type Ia supernovae (SNIa), which serve as the major source of iron, in the creation of the bimodality. To this end, we divide SNIa into two groups, those formed from the 1st generation stars (the first SNIa) and those formed from the 2nd generation stars (the second SNIa). The model with the first SNIa suppressed during the *second* star formation stage produces stars having high $[\alpha/\text{Fe}]$ in the early phase of this stage, whereas the model which prohibits the second SNIa produces high $[\alpha/\text{Fe}]$ stars in the late phase. Both models fail to create a well-defined bimodality. We thus conclude that the cooperation of the first and the second SNIa plays a crucial role in creating the bimodality by maintaining rich iron content in the interstellar gas throughout the second star formation stage.

Key words: Galaxy:formation – Galaxy:disc – Galaxy:abundance – galaxies: formation

1 INTRODUCTION

Detailed spectroscopic studies in recent years suggest the existence of two distinct types of stars with different chemical compositions in the Milky Way disc (e.g. [Adibekyan et al. 2012](#); [Haywood et al. 2013](#); [Bensby, Feltzing & Oey 2014](#); [Hayden et al. 2015](#)). This bimodality is most clearly represented in the distribution of long-lifetime stars in the abundance diagram which plots $[\alpha/\text{Fe}]$ ratio against $[\text{Fe}/\text{H}]$. Although this phenomenon is one of the most notable chemical properties characterizing the Milky Way and should give an important clue to the formation process of MW, its origin remains a long-standing riddle. In order to tackle this problem, [Chiappini, Matteucci & Gratton \(1997\)](#) devised a phenomenological model, in which the gas infall comprising two distinct episodes is specified. This approach is also taken in a recent modelling by [Spitoni et al. \(2019\)](#), which gives a fair reproduction of the observed abundance pattern. Recent studies by [Lian et al. \(2020a,b\)](#) also discuss the bimodal abundance distributions and construct chemical evolution models involving two gas accretion events to explain them. In these studies, however, the gas infall history is given by particularly parameterized formula and the best model is searched by adjusting model parameters. Therefore, the fundamental mechanism that underlies the creation of the chemical bimodality remains unclear.

[Noguchi \(2018\)](#) showed that the cold accretion hypothesis, which is deduced from recent large-scale cosmological simulations, naturally implies a two-stage gas accretion, giving one promising solution to this problem. These simulations (e.g.

[Fardal et al. 2001](#); [Keres et al. 2005](#); [Dekel & Birnboim 2006](#); [Ocvirk, Pichon & Teyssier 2008](#); [van de Voort & Schaye 2012](#); [Nelson et al. 2013](#)) trace the thermal history of the cosmic gas as it is incorporated into growing dark matter halos in the cold dark matter universe using hydrodynamical code. Specifically, in most of these simulations, the gas component experiences adiabatic heating and cooling, shock heating, inverse Compton cooling off the microwave background, and radiative cooling via free-free emission, collisional ionization and recombination, and collisionally excited line cooling. Those simulations provide the most realistic picture of the thermal and dynamical properties of the halo gas in forming galaxies, thereby serving as the best starting point for examining the further evolution of the baryon content in individual galaxies. A particularly important finding of these numerical works is that the cosmic gas captured by dark matter halos accretes to the forming galaxies without being heated-up by shock waves as envisaged in the classical picture (e.g. [Rees & Ostriker 1977](#)), but in unheated states when the halos are not massive enough (namely, cold accretion). This finding has a large impact on various aspects of galaxy evolution, especially in its early stage ([Dekel et al. 2009](#)). The spirit of [Noguchi \(2018\)](#) was to apply this cold-accretion hypothesis to MW and to interpret chemical properties of individual stars as we observe today in a cosmological perspective.

In the cold-accretion paradigm, the shift of the gas accretion mode as the halo grows in mass leads to the separation of the galactic star formation process into two stages ([Noguchi 2018](#)). Initially, the cold-mode gas accretion causes a rapid star formation for a couple of Gyrs (the first SF), leaving stars containing copious α -elements synthesized by type II supernovae (SNII). When the accretion process is switched

★ E-mail: noguchi@astr.tohoku.ac.jp (MN)

to the cooling flow of the shock-heated halo gas (the hot mode) (e.g. [Rees & Ostriker 1977](#)), the second episode of star formation (the second SF) starts, continuing to the present epoch. During this phase, iron-rich stars are formed. The gap between the free-fall time and the radiative cooling time causes a dormant period between two phases, in which the gas accretion is much suppressed. Such a possibility is also suggested by [Birnboim, Dekel & Neistein \(2007\)](#) in their spherical accretion models without star formation.

[Noguchi \(2018\)](#) succeeded in reproducing the stellar abundance distribution broadly consistent with the observational data for the solar neighbourhood (e.g. [Haywood et al. 2013](#)) as well as the inner and outer discs of MW obtained by the APOGEE project ([Majewski et al. 2017](#)). These global features over the wide area of MW are manifested more clearly in the most recent APOGEE DR16 data ([Queiroz et al. 2020](#)) showing the bimodality now extending towards the innermost regions, lending further credence to the scenario of [Noguchi \(2018\)](#). Moreover, this scenario may also be applicable to other disc galaxies in general. Indeed, M31, the most massive disc galaxy in the Local group, has a hint of two-stage star formation as revealed by color-magnitude diagram analysis of individual stars ([Williams et al. 2017](#)). Stellar population synthesis applied to a number of MW-sized disc galaxies ([Gonzalez Delgado et al. 2017](#)) also suggests the existence of two star formation episodes in those galaxies. These observational studies seem to give a further support to the picture of massive disc galaxy evolution given in [Noguchi \(2018\)](#), suggesting its universality beyond MW.

Although [Noguchi \(2018\)](#) proposes a promising scenario to explain the observational data, the key mechanism underlying the bimodality is yet to be clarified. In [Noguchi \(2018\)](#), the high $[\alpha/\text{Fe}]$ metal-poor stellar population formed in the first SF is reasonably explained as the result of relatively rapid star formation which ends before SNIa start to explode massively. It was observed in the simulation that the interstellar gas in the second SF epoch remains constantly low in $[\alpha/\text{Fe}]$ ratio and this fact was used to explain the formation of a low $[\alpha/\text{Fe}]$ metal-rich population distinct from the first stellar group, namely a bimodality. Although the low $[\alpha/\text{Fe}]$ status in the second SF epoch is essential in creating a bimodality, how such a state is realized was not clarified. Another unsolved problem is what influence the gas which remains after the first SF is over has on the gas metallicity in the second SF epoch. The remaining gas will mix the fresh gas supplied by the second accretion and may have non-negligible influence on the gaseous metal content in the second SF epoch.

Type Ia supernovae (SNIa) are believed to be the main supplier of iron in the interstellar gas (for recent references, e.g. [Chiappini, Matteucci & Gratton 1997](#); [Haywood et al. 2013](#); [Hayden et al. 2015](#)). In the model of [Noguchi \(2018\)](#), SNIa are produced in both the first and the second SF episodes and both of these SNIa groups can affect the metallicity of the interstellar gas and the stars that formed from it in the second SF epoch. Because such a grouping of SNIa associated with the separation of star formation into two distinct epochs is a unique situation only realized in the cold-accretion paradigm, it is worthwhile to scrutinize the role played by each SNIa group in the emergence of the chemical bimodality. To this end, we divide SNIa into two groups according to the birth epoch of their progenitors and employ a suite of evolution models, in some of which the effect of either SNIa group is artificially switched-off. The fiducial model is essentially the same as the model adopted in [Noguchi \(2018\)](#). By intercomparing their behaviour, we can clarify how the two groups cooperate in keeping the high iron abundance throughout the second stage and thus creating a well-defined bimodality.

Section 2 gives a brief description of the models, while the main results are given in section 3. Section 4 discusses the limitation of the present work and conclusions are summarized in section 5.

2 MODELS

We use the same evolution code as employed in [Noguchi \(2018\)](#). Briefly, we divide the whole galactic disc into a series of concentric annuli and calculate the evolution of each ring under the accretion of gas from the halo. The cooling rate of the gas which determines the accretion rate is calculated assuming the collisional ionization equilibrium. The prediction based on the cold accretion theory ([Dekel & Birnboim 2006](#)) is used to set the epoch dividing the early cold-accretion phase and the late cooling-flow phase. In the former phase, the halo gas is assumed to accrete to the disc plane with the free-fall time, while the gas accretes with the radiative cooling timescale in the later phase. The accreting gas is assumed to be pristine (i.e., free of any metals). It should be noted that, as stated in section 1, the accretion history thus determined is based on the results of detailed cosmological simulations for the CDM scenario (e.g. [Fardal et al. 2001](#); [Keres et al. 2005](#); [Dekel & Birnboim 2006](#); [Ocvirk, Pichon & Teyssier 2008](#); [van de Voort & Schaye 2012](#); [Nelson et al. 2013](#)), which provide reliable thermal history of the cosmic gas, so that the time-scales and intensities of the two infall episodes, and time gap between them are automatically determined with sufficient physical ground.

We include the star formation process from the accreted gas (i.e., interstellar gas), the energy injection and metal enrichment from SNII and SNIa. The former explode instantly when their progenitors are formed and return $3.81 M_{\odot}$ of α -elements and $0.094 M_{\odot}$ of iron. These are the yields per one SNII averaged over the Salpeter initial mass function. SNIa explodes with a certain delay which is specified by the delayed time distribution (DTD) taken from [Maoz, Sharon & Gal-Yam \(2010\)](#),

$$\text{DTD}(t) = 1 \times 10^{-3} \text{SN Gyr}^{-1} M_{\odot}^{-1} t^{-1.1}$$

where t denotes the time in Gyr that elapsed since the progenitor formed. We assume that $\text{DTD}=0$ for $t < 0.3$ Gyr. [Maoz, Sharon & Gal-Yam \(2010\)](#) favoured the minimum delay time of 0.1 Gyr based on the galaxy cluster data, while [Homma et al. \(2015\)](#) found that adoption of 0.5 Gyr best reproduces the $[\alpha/\text{Fe}]$ - $[\text{Fe}/\text{H}]$ diagrams of the local dwarf spheroidal galaxies. The present minimum delay time of 0.3 Gyr is the mean of these two values. Each SNIa returns $0.438 M_{\odot}$ of α -elements and $0.63 M_{\odot}$ of iron. Thus, SNII are the main source for α -elements while iron is mostly provided by SNIa. The α -yield for SNII and iron-yield for SNIa used here are respectively increased by 20 percent and decreased by 15 percent from the yields given in [Ferreras & Silk \(2002\)](#), which themselves are based on [Thielemann, Nomoto & Hashimoto \(1996\)](#) for SNII and [Thielemann, Nomoto & Yokoi \(1986\)](#) for SNIa. These minor changes are within the estimated uncertainties in the current stellar evolution models (e.g. [Romano et al. 2010](#)), and do not affect any conclusions of the present study.

In order to mimic MW, we choose the present virial mass of the halo, $M_{\text{vir}} = 1.23 \times 10^{12} M_{\odot}$. Setting the supernova feedback efficiency to $\varepsilon = 0.15$ leads to the disc size and mass nearly consistent with the observed values for MW ([Noguchi 2018](#)). We consider the annulus with $7\text{kpc} < r < 9\text{kpc}$, where r is the galactocentric distance, as a representative region for the solar neighbourhood. Fig.1 shows the gas accretion history for this selected region. In this MW-analog,

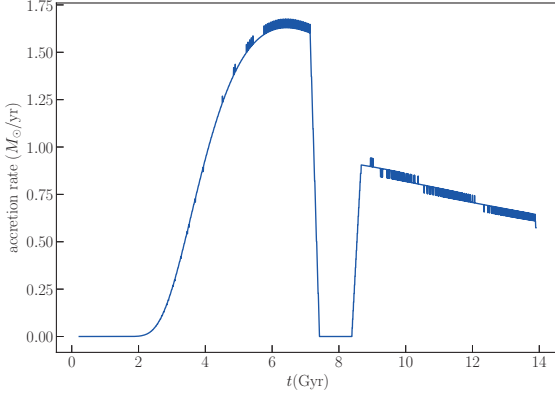


Figure 1. Gas accretion rate plotted against the cosmological time, t . All the models studied in this work have the same accretion history. The running mean over 40 successive time steps (0.28 Gyr) is plotted to suppress the short timescale fluctuations arising in the model calculation.

Table 1. Model setting.

Model	SNIa(1st)	SNIa(2nd)	metal reset	gas reset
1(fiducial)	Yes	Yes	No	No
2	No	Yes	No	No
3	Yes	No	No	No
4	Yes	Yes	Yes	No
5	Yes	Yes	Yes	Yes

the rapid free-fall accretion (i.e., cold-mode accretion) continues up to ~ 8 Gyr, after which it is taken over by the cooling flow, continuing to the present epoch. Because of the gap in the accretion timescale at the transient epoch, a hiatus about 1 Gyr long appears after the end of cold accretion. Detailed mechanism for this two-stage accretion is discussed in [Noguchi \(2018\)](#).

We run one fiducial model and four artificial models with different settings for the included processes as summarized in table 1. They are classified according to two kinds of options. First is if the metal enrichment by the first and/or second SNIa is included in the second epoch (i.e. $t > 8.6$ Gyr) or not (2nd and 3rd columns). The first SNIa here is defined as those SNIa originating in the stars formed in the first epoch of star formation (before $t=8.6$ Gyr). The second SNIa refers to those SNIa formed from the second generation stars created after $t=8.6$ Gyr. Second option is if the metal content (α elements and iron) in the interstellar gas or the entire gas (including metals) is removed or not at the beginning of the second gas accretion (i.e. $t=8.6$ Gyr) (3rd and 4th columns). Note that the fiducial model is essentially the same as the model discussed in [Noguchi \(2018\)](#).

3 RESULTS

Before detailed discussion of the present results, we first show the distribution of the abundance ratios of the fiducial model (Model 1) in Fig.2 and compare it with the observation for the solar neighbourhood by the APOGEE project ([Majewski et al. 2017](#)). Incidentally, this model gives the present star formation rate density of $3.2 \times 10^1 M_\odot/\text{Gyr}/\text{pc}^2$ for the solar neighbourhood. The model produces two distinct stellar groups, one with high $[\alpha/\text{Fe}]$ and low $[\text{Fe}/\text{H}]$

and another with low $[\alpha/\text{Fe}]$ and high $[\text{Fe}/\text{H}]$ in agreement with the APOGEE observation and other several observational results (e.g. [Adibekyan et al. 2012](#); [Bensby, Feltzing & Oey 2014](#); [Hayden et al. 2015](#); [Haywood et al. 2016](#)). The peak locations of respective groups and the total $[\alpha/\text{Fe}]$ distribution are in reasonable agreement with the observations considering the idealized nature of the present evolution model. Some discrepancy is seen for more detailed features. The model does not develop two parallel sequences for $[\text{Fe}/\text{H}] > 0.3$ so clearly as reported by [Nissen et al. \(2020\)](#), with its α -rich branch too weak for this metallicity range. Recent observations (e.g. [Silva Aguirre et al. 2018](#)) show overlap also in $[\alpha/\text{Fe}]$ ratios and stellar ages of the two groups that the present model does not produce (the latter by construction). Some recent studies (e.g. [Spitoni et al. 2019](#)) try to reproduce these detailed features by exploring the parameter space of the chemical evolution models to obtain the best fit values. In contrast to these studies, the aim of the present study is to clarify the most basic mechanism underlying the chemical bimodality in the framework of the cold accretion theory implied by the CDM cosmology. This issue has not been the subject of intensive studies so far. In this spirit, this study does not aim to reproduce every detail of the observed abundance patterns and we define the bimodality as the existence of two distinct stellar groups, one having high $[\alpha/\text{Fe}]$ and low $[\text{Fe}/\text{H}]$ and another having low $[\alpha/\text{Fe}]$ and high $[\text{Fe}/\text{H}]$ at the locations in the abundance diagram approximately consistent with the observed ones. It is noted that the bimodality defined in this way persists in the most recent APOGEE DR16 observations ([Queiroz et al. 2020](#)).

As discussed intensely in the literature (e.g. [Chiappini, Matteucci & Gratton 1997](#); [Haywood et al. 2013](#); [Hayden et al. 2015](#)), the production of iron by SNIa is regarded as the essential ingredient bringing about chemical diversity, especially the iron content, in the formed stars. Because of their delayed response to the star formation events, a rapid star formation generally leads to the production of stars with high $[\alpha/\text{Fe}]$ ratios due to poor iron content in the parent interstellar gas. In contrast, a slow star formation with a longer timescale than the delay time produces high $[\alpha/\text{Fe}]$ stars in early times but starts to create iron-rich stellar populations as SNIa explosions become frequent.

In the fiducial model (Model 1), the first SF fuelled by the cold accretion produces an α -element rich stellar population, while the second SF driven by the cooling-flow produces iron-rich stars. These processes create the two stellar groups well-separated in the $[\alpha/\text{Fe}]-[\text{Fe}/\text{H}]$ plane as shown in Figs.2 and 3a. Delayed explosions of SNIa with respect to SNII result into a relatively low ratio of the SNIa rate to the SNII rate until the SFR reaches a maximum in the first stage ($t \sim 7.5$ Gyr, Fig.3b), while, in the second stage, this ratio rises as the SNIa events catch up with SNII explosions (the peak ratio at the transition epoch, $t \sim 8.6$ Gyr, can be neglected because of its short duration). This process is reflected in the time variation of elemental abundances plotted in Fig.3c. The interstellar gas has a high $[\alpha/\text{Fe}]$ ratio before $t \sim 8$ Gyr, whereas this ratio stays at a low level in the second epoch. Because the decline of this ratio is abrupt and takes place at the period where SFR is low due to the temporal pause of the gas accretion, there appears a gap in the $[\alpha/\text{Fe}]$ distribution between the first and second stellar groups.

We examine in more detail the role of SNIa in creating this bimodality by comparing the result of Model 1 with those of Models 2 and 3, which have different SNIa treatments.

In Model 2, the first SNIa are prohibited to explode in the second stage (i.e., after $t=8.6$ Gyr). In this case, the SNIa rate and the SNIa/SNII ratio in the beginning of the second episode are both low, being contributed only by the second SNIa (Fig.3e). Therefore, the

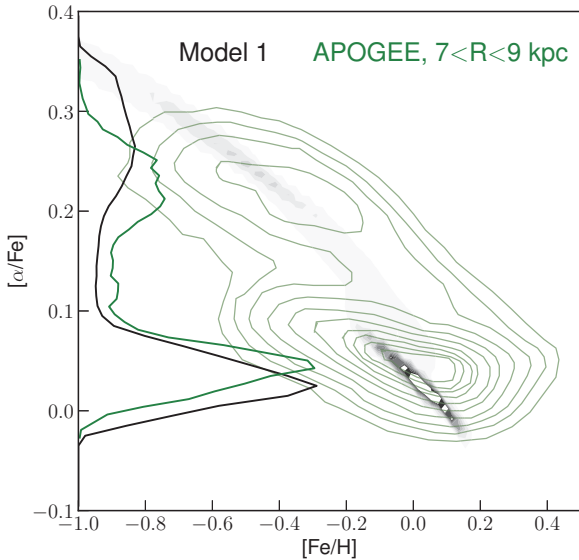


Figure 2. Fiducial model compared with the observational data. The abundance distribution of the model is indicated by the gray scale image whereas green contours show the distribution for the solar neighbour stars obtained by APOGEE (Haywood et al. 2016). The histograms on the left axis show the distribution of $[\alpha/\text{Fe}]$ for the model (black) and the observation (green), normalized so that the integrated area is equal.

$[\text{Fe}/\text{H}]$ ratio remains smaller than that in the fiducial model (Fig.3f). Because $[\alpha/\text{H}]$ stays at a high level from the outset due to quick replenishment of α -elements from the second SF (Fig.3e), $[\alpha/\text{Fe}]$ increases during early few Gyrs in the second stage (Fig.3f). Although the delayed iron enrichment from the second SNIa lowers $[\alpha/\text{Fe}]$ in the late phase, the lack of contribution from the first SNIa and resulting high $[\alpha/\text{Fe}]$ ratios during the early phase bury the gap between the first and second populations in the abundance diagram (Fig.3d), leading to an almost continuous sequence. Although the histogram in Fig.3d may indicate a bimodality in $[\alpha/\text{Fe}]$, the gray scale map shows that the bimodality in this model is significantly degraded compared with that in the fiducial model. This is because the two peaks in the $[\alpha/\text{Fe}]$ distribution are more closely located and the second generation stars exhibit a broader distribution. Model 2 thus demonstrates that the iron enrichment from the first SNIa extending into the second stage is indispensable in establishing a well-defined bimodality.

Then what about the role of the second SNIa? Model 3 was run with the effect of the second SNIa totally cutoff, but the first SNIa are allowed to explode throughout the whole calculated period. In this case, the stars formed in the early phase of the second epoch have low $[\alpha/\text{Fe}]$ values owing to the delayed action of the first SNIa, leading to their location well-separated from the first stellar group as seen in Fig.3g. In the later phase, however, RSNi and hence the SNIa/SNII ratio decrease (Fig.3h) as the contribution from the first SNIa decays with no subsequent replacement from the second SNIa. As a result, the $[\alpha/\text{Fe}]$ ratio returns back to high values (Fig.3i), leading to a quite different abundance pattern from the fiducial model (Fig.3g). This demonstrates that the first SNIa alone cannot produce the bimodality.

In summary, the first SNIa contribute to maintain $[\alpha/\text{Fe}]$ low in the early phase of the second SF, whereas the second SNIa keep the low level of $[\alpha/\text{Fe}]$ in the later half of the second SF period. The two SNIa

groups thus cooperate to keep $[\alpha/\text{Fe}]$ sufficiently low throughout the second SF, leading to a well-defined bimodality.

Another interesting question is to what degree the interstellar gas remaining at the dormant period contributes to the establishment of the chemical bimodality. As shown in Fig.3, considerable amount of the interstellar gas (with the gas fraction $f_g \sim 50$ percent) remains after the first SF is over, which contains copious iron and has a low $[\alpha/\text{Fe}]$ ratio. If this remaining gas is completely turned into stars, they would occupy a non-negligible portion of the total second stellar population and affect its abundance ratio. The low $[\alpha/\text{Fe}]$ of the second generation stars thus may simply come from the abundance pattern of this remaining interstellar gas.

In order to explore this possibility, Model 4 was run with the abundances of α -elements and iron reset to zero at $t=8.6$ Gyr, i.e., the beginning of the second SF (Table 1). In other words, the interstellar gas is preserved but it is now pristine. As shown in Fig.4d, this model produces a well-defined bimodality similar to the one in the fiducial model (Fig.4a). In this model, the second SF quickly lifts up the $[\alpha/\text{H}]$ ratio as indicated in Fig.4f. However, the iron production by the first SNIa continuing from the first episode promptly rises the interstellar $[\text{Fe}/\text{H}]$ as well. The vestige of gas 'purification' applied at $t=8.6$ Gyr is quickly erased. Therefore, the chemical enrichment history in the second episode of this model is essentially the same as that in the fiducial model, and the $[\alpha/\text{Fe}]$ ratio is low from the early phase of this episode as shown in Fig.4f.

Model 5 embodies a more extreme situation, in which the whole remaining interstellar gas is removed at the beginning of the second episode (Fig.4h). This model also produces a clear bimodality in the abundance diagram (Fig.4g), although details are different from the fiducial model. Amount of the second generation stars is reduced because of the gas removal and a long tail extends to very low $[\alpha/\text{Fe}]$ ratios from the clump of the second generation stars. Despite these subtle differences, Fig.4i reveals essentially the same enrichment history of this model as those of Models 1 and 4. The second episode of Model 5 is regarded as just another isolated gas accretion and star formation event independent upon the outcome of the preceeding first episode *except* that the first SNIa are existent from the outset. By its own, such a single star formation event would produce high $[\alpha/\text{Fe}]$ stars in the beginning, with this ratio decreasing continuously as the star formation proceeds. In Model 5, however, the extant first SNIa act to lower $[\alpha/\text{Fe}]$ ratio of the second generation stars from the beginning and no α -element rich stars are produced (Fig.4i). Thus a chemical bimodality is created in fundamentally the same way as in the fiducial model. By these experiments, we can conclude that the gas remaining after the first SF plays at most a secondary role in establishing the chemical bimodality.

4 DISCUSSION

We briefly discuss the limitation of the current study. Here, we did not explore a large domain in the parameter space but considered several variations around the fiducial model which is plausible for the currently observable regions of the MW disc. Although this approach is adequate for the present purpose, it should be cautioned that the above argument concerning the emergence of the bimodality in the presence of two separated gas accretion episodes may not necessarily apply to other regions of the MW disc or other disc galaxies. If, for example, the time-lag between the two star formation episodes is much larger than the decay timescale of SNIa, then the importance of the first SNIa in the second episode will be much reduced, and the entire chemical pattern of the disc stars will be just the superposition

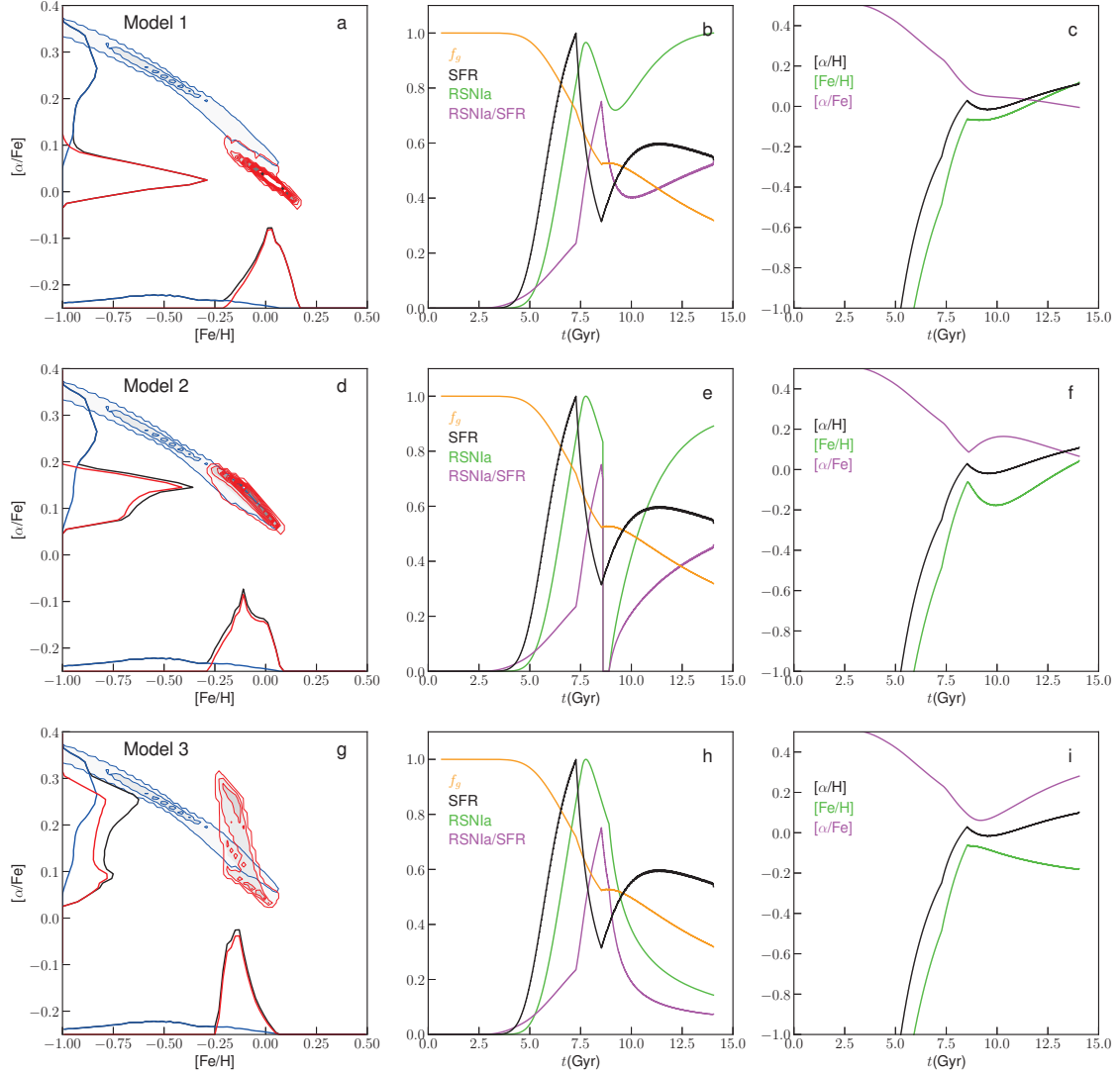


Figure 3. Stellar abundance distributions (Panels a,d, and g), the time development (Panels b,e, and h), and the chemical enrichment (Panels c,f, and i) for Models 1 (upper), 2 (middle), and 3 (bottom). In the left panels, the blue and red contours (equally spaced in linear scale) respectively indicate the stellar density for the first and second stellar groups divided at $t = 8.6$ Gyr, with the total density distribution shown in gray scale. The blue and red histograms on the left axis indicate the $[\alpha/\text{Fe}]$ distribution for the corresponding groups while the black histogram indicates the total. The histograms on the bottom axis indicate the distribution of $[\text{Fe}/\text{H}]$ in the same manner. In the centre panels, the gas fraction is calculated as $f_g \equiv m_g/(m_g + m_s)$ from the interstellar gas mass, m_g , and the stellar mass, m_s . The rates of the star formation (SFR) and SNIa (RSN Ia) are normalized by their maximum values. Ratio of the RSN Ia and SFR is given in an arbitrary unit but its normalization is common to the three indicated models to facilitate comparison.

of the patterns made by two independent star formation episodes. The large overlapping of the two patterns expected in such a case will destroy the bimodality.

Is it possible that such a situation takes place in reality? In this regard, models with more massive virial masses provide useful information because the gap duration tends to increase for more massive galaxies. A model with $M_{\text{vir}} = 2.48 \times 10^{12} M_{\odot}$ was run to examine

this point. This model has a gap duration ~ 2 Gyr, about twice that in the fiducial model. With all other parameters fixed the same as in the fiducial model, the shift in $[\alpha/\text{Fe}]$ for the two stellar populations increased from ~ 0.2 to ~ 0.3 , although the stellar distribution on $[\alpha/\text{Fe}]$ - $[\text{Fe}/\text{H}]$ diagram remains qualitatively the same, showing a clear bimodality. The present total stellar mass in this model is $1.05 \times 10^{11} M_{\odot}$, nearly at the upper limit for the observed disc

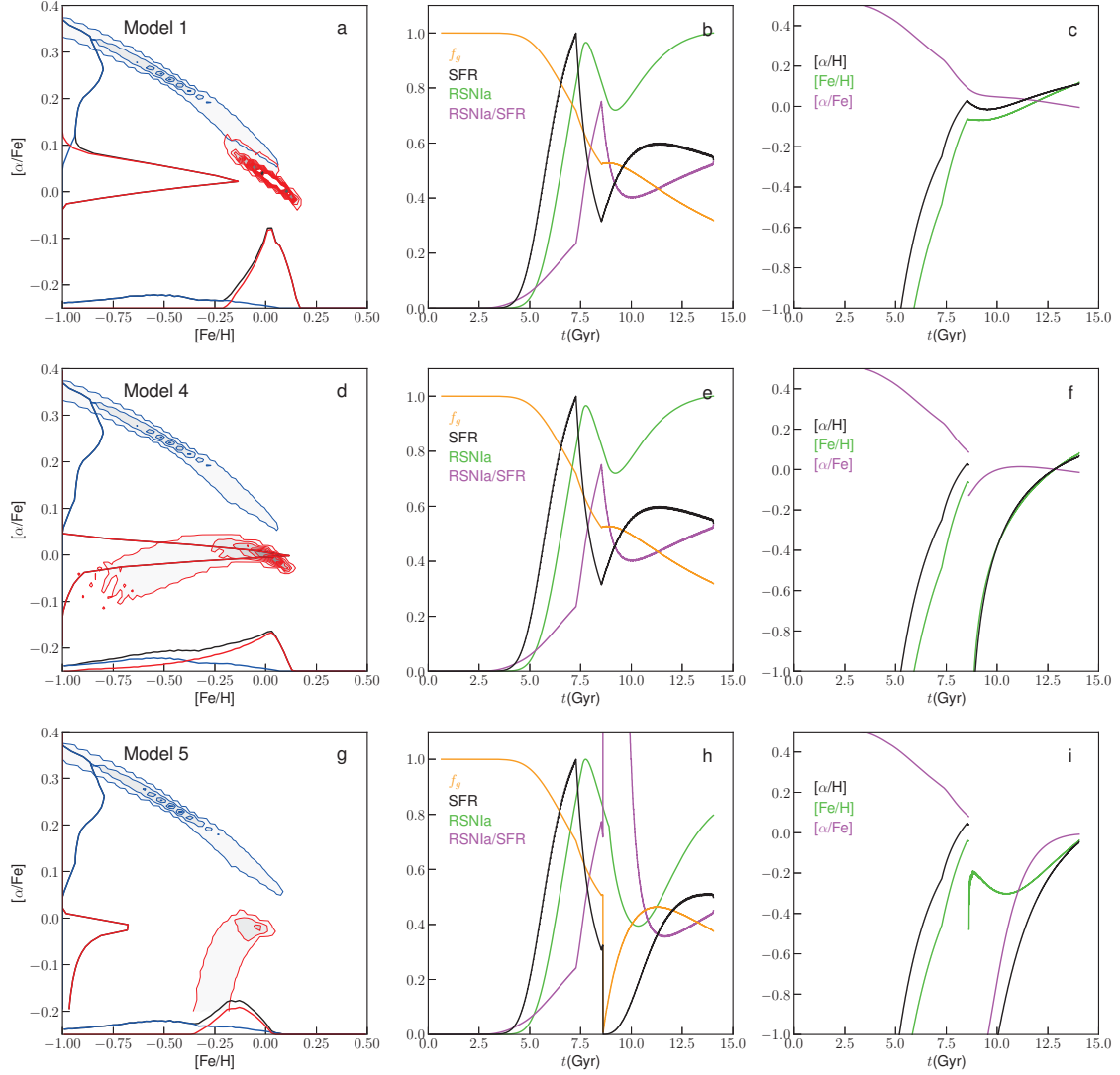


Figure 4. Same as Fig.3 but for Models 1 (upper), 4 (middle), and 5 (bottom).

masses. Therefore, there is little possibility that a too large accretion gap results into two overlapping stellar distributions in the abundance diagram. This more massive model likely represents M31 in the Local Group, for which a longer star formation gap than that for MW is actually inferred from the color-magnitude diagram dating of individual stars (Williams et al. 2017). Future observation of the abundance pattern for this nearby galaxy would be interesting, providing a powerful diagnostics for the cold accretion model for galactic chemical evolution.

Another situation is the case in which the second episode of gas accretion dominates the first one. In this case, the stellar population formed in the second episode outnumbers the first one, and the whole

evolution approaches to that of a single star formation event. The outcome is an elongated stellar distribution in the $[\alpha/\text{Fe}]$ - $[\text{Fe}/\text{H}]$ diagram (running from the upper left to the lower right) made by the second generation stars with a negligible contribution from the first generation. This situation actually occurs in the far-out region of the MW disc, for example. Indeed, the abundance diagram for the outermost region ($11\text{kpc} < r < 13\text{kpc}$) shown in Noguchi (2018) exhibits such stellar distribution, in agreement with the observations for the corresponding regions of the MW disc (Hayden et al. 2015; Queiroz et al. 2020).

Bearing in mind the applicability of this cold-accretion-based scenario to other nearby galaxies, a preliminary attempt was made in

Noguchi (2018) to clarify the dependence of star formation history on the mass of the host galaxy as partly mentioned above. Figuring out the necessary and sufficient conditions to ensure a clear bimodality is desired also in view of a large variety in the properties (the halo virial mass, the stellar and gaseous masses, the star formation history, etc) of the Local Group disc galaxies (e.g. Williams et al. 2009; Gogarten et al. 2010; Williams et al. 2017).

Finally, putting aside these theoretical issues regarding the global properties of the bimodality, the cause of several discrepancies between the present model and the solar neighbourhood observation in detailed features deserves further exploration. For example the present study does not attempt to explain the $[\alpha/\text{Fe}]$ poor metal-poor population observed in the solar neighbourhood (e.g. Adibekyan et al. 2012; Bensby, Feltzing & Oey 2014). This population most likely resulted from the migration and mix of stars born at different galactocentric distances (e.g. Schonrich & Binney 2009). Although the present code, which calculates the evolution of individual annular disc regions independently on other regions, does not permit the inclusion of the radial migration of disk material, its effect on the resultant chemical abundance pattern of the disc stars should be further explored before the chemical evolution of MW disc is fully understood. Such studies will not only provide additional constraints on the galaxy formation scenarios but also contribute to improve stellar evolution models.

5 CONCLUSIONS

The whole process envisaged for the creation of chemical bimodality in the MW disc stars is summarized as follows. The change of the gas accretion from the cold mode to the hot mode as MW grows in mass induces division of the star formation process into two stages. In the first stage, the termination of the cold-mode accretion before the massive occurrence of SNIa leaves behind a stellar population relatively rich in α -elements. In the second stage of star formation driven by the cooling flow, the interstellar gas is effectively polluted by iron ejected by the SNIa formed from the 1st generation stars in its early epoch whereas the SNIa originating in the 2nd generation stars mainly contribute to iron enrichment in its late epoch. This ceaseless supply of iron maintains the iron abundance in the interstellar gas at a sufficiently high level throughout the entire second stage, so that the 2nd generation stars constitute an α -poor and iron-rich stellar population well separated from the first generation stars in the $[\text{Fe}/\text{H}]$ - $[\alpha/\text{Fe}]$ plane.

ACKNOWLEDGEMENTS

We thank the anonymous referee for useful comments which helped us improve the paper.

Data availability

The data underlying this article will be shared on reasonable request to the corresponding author.

REFERENCES

- Adibekyan V. Zh. et al., 2012, *A&A*, 545, 32
 Bensby T., Feltzing S., Oey M. S., 2014, *A&A*, 562, 71
 Birnboim Y., Dekel A., Neistein E., 2007, *MNRAS*, 380, 339
 Chiappini C., Matteucci F., Gratton R., 1997, *ApJ*, 477, 765

- Dekel A., Birnboim Y., 2006, *MNRAS*, 368, 2
 Dekel A. et al., 2009, *Nature*, 457, 451
 Fardal M. A. et al., 2001, *ApJ*, 562, 605
 Ferrarar L., Silk J., 2002 *MNRAS*, 336, 1181
 Gogarten S.M. et al., 2010, *ApJ*, 712, 858
 Gonzales Delgado R.M. et al., 2017, *A&A*, 607, A128
 Hayden M. R. et al., 2015, *ApJ*, 808, 132
 Haywood M. et al., 2013, *A&A*, 560, 109
 Haywood M. et al., 2016, *A&A*, 589, 66
 Homma H. et al., 2015, *ApJ*, 799, 230
 Keres D. et al., 2005, *MNRAS*, 363, 2
 Lian J. et al., 2020a, *MNRAS*, 494, 2561
 Lian J. et al., 2020b, *MNRAS*, 497, 2371
 Majewski S.R. et al., 2017, *AJ*, 154, 94
 Maoz D., Sharon K., Gal-Yam, A., 2010, *ApJ*, 722, 1879
 Nelson D. et al., 2013, *MNRAS*, 429, 3353
 Nissen P. E. et al., 2020, *A&A*, 640, 81
 Noguchi M., 2018, *Nat*, 559, 585
 Ocvirk P., Pichon C., Teyssier R., 2008, *MNRAS*, 390, 1326
 Queiroz A.B.A. et al., 2020, *A&A*, 638, A76
 Rees M. J., Ostriker J. P., 1977, *MNRAS*, 179, 541
 Romano D. et al., 2010, *A&A*, 522, 32
 Schonrich R., Binney J., 2009, *MNRAS*, 399, 1145
 Silva Aguirre V. et al., 2018, *MNRAS*, 475, 5487
 Spitoni E. et al., 2019, *A&A*, 623, 60
 Thielemann F., Nomoto K., Hashimoto M., 1996, *ApJ*, 460, 408
 Thielemann F., Nomoto K., Yokoi K., 1986, *A&A*, 158, 17
 van de Voort F., Schaye J., 2012, *MNRAS*, 423, 2991
 Williams B.F. et al., 2009, *ApJ*, 695, L15
 Williams B.F. et al., 2017, *ApJ*, 846, 145

This paper has been typeset from a \LaTeX file prepared by the author.